Opening the $Co^{III,IV}_2(\mu\text{-}O)_2$ Diamond Core by Lewis Bases Leads to Enhanced C–H Bond Cleaving Reactivity

Yan Li,[1] Suhashini Handunneththige,[2] Jin Xiong,[3] Yisong Guo,[3]* Marat R. Talipov[2]* and Dong Wang[1]*

[1] Department of Chemistry and Biochemistry, Center for Biomolecular Structure and Dynamics, University of Montana, Missoula, MT 59803, USA

[2] Department of Chemistry and Biochemistry, New Mexico State University, Las Cruces, New Mexico 88003, United States

[3] Department of Chemistry, Carnegie Mellon University, Pittsburgh, PA 15213, USA

ABSTRACT: The high-valent diiron(IV) intermediate **Q** is the key oxidant that cleaves strong C–H bonds of methane in the catalytic cycle of soluble methane monooxygenase (sMMO). sMMO-**Q** was previously reported as a bis-μ-oxo $Fe^{IV}_2(\mu\text{-}O)_2$ diamond core but recently described to have an open core with a long Fe•••Fe distance. We recently reported a high-valent $Co^{III,IV}_2(\mu\text{-}O)_2$ diamond core complex (**1**) that is highly reactive with sp^3 C–H bonds. In this work, we demonstrated that the C–H bond cleaving reactivity of **1** can be further enhanced by introducing a Lewis base X, affording faster kinetic rate constants and the ability to cleave stronger C–H bonds compared to **1**. We proposed that **1** first reacts with X in a fast equilibrium to form an open core species $X–Co^{III}–O–Co^{IV}–O$ (**1-X**). We were able to characterize **1-X** using EPR spectroscopy and DFT calculations. **1-X** exhibited an $S = 1/2$ EPR signal distinct from that of the parent complex **1**. DFT calculations showed that **1-X** has an open core with the spin density heavily delocalized in the $Co^{IV}–O$ unit. Moreover, **1-X** has a more favorable thermodynamic driving force and a smaller activation barrier than **1** to carry out C–H bond activation reactions. Notably, **1-X** is at least four orders of magnitude more reactive than its diiron open core analogs. Our findings indicate that the diamond core isomerization is likely a practical enzymatic strategy to unmask the strong oxidizing power of sMMO-**Q** necessary to attack the highly inert C–H bonds of methane.

Introduction.

The diiron active site in nonheme metalloenzyme soluble methane monooxygenase (sMMO) activates dioxygen and produces a high-valent diiron(IV) intermediate **Q**, one of nature's strongest oxidants, to cleave inert C–H bonds of methane (bond dissociation energy, BDE = 105 kcal/mol) and selectively form the hydroxylated product methanol.[1-2] It has become a frontier research in recent years to investigate the nature of sMMO-**Q** using spectroscopic, computational and biomimetic/bio-inspired approaches.[1] The structure of sMMO-**Q** was previously described as a bis-μ-oxo bridged $Fe^{IV}_2(\mu\text{-}O)_2$ diamond core based on evidence obtained from Mossbauer spectroscopy, X-ray absorption spectroscopy (XAS) and resonance Raman spectroscopy.[3-6] However, recent work by DeBeer et al. using high-energy-resolution fluorescence detected X-ray absorption spectroscopy (HERFD XAS) argued against the diamond core assignment, and claimed that sMMO-**Q** has an open core structure with a long Fe•••Fe distance of ~3.4 Å.[7-8]

A number of studies by Nam, Goldberg and others have shown that the reactivities of synthetic mononuclear iron-oxo and manganese-oxo complexes can be tuned by neutral or anionic axial ligands in both heme and nonheme systems.[9-14] Furthermore, recent studies of a high-valent $Fe^{III,IV}_2(\mu\text{-}O)_2$ model complex showed that the bis-μ-oxo bridged diamond core interacts with a Lewis base to form an open core species with a terminal Fe^{IV}=O moiety.[15-17] The open core species exhibited a million-fold rate enhancement for C–H bond activation.[17]

Very recently, we reported a novel high-valent $Co^{III,IV}_2(\mu\text{-}O)_2$ diamond core complex (**1**) supported by neutral tetradentate tris(2-pyridylmethyl)amine (TPA) ligand (structure shown in Figure 2).[18] Complex **1** has a short Co•••Co distance of 2.78 Å and an $S = 1/2$ ground state having spin delocalization on both cobalt centers. Notably, **1** is highly reactive with hydrocarbons and cleaves sp^3 C–H bonds 3-5 orders of magnitude faster than diiron and dimanganese diamond core analogs. In this work, we demonstrated that the C–H bond cleaving reactivity of **1** can be further enhanced by introducing a Lewis base X, affording faster kinetic rate constants and the ability to cleave stronger C–H bonds up to 96 kcal/mol compared to **1**. We proposed that **1** first reacts with X in a fast equilibrium to form an open core species $X–Co^{III}–O–Co^{IV}–O$ (**1-X**). We were able to measure the equilibrium constant for this reaction and trap **1-X** for its characterization by electron paramagnetic resonance (EPR) spectroscopy. **1-X** exhibited an $S = 1/2$ EPR signal with clearly detectable ^{59}Co nuclear hyperfine splittings at X-band frequency, which is distinct from that of the parent diamond core complex **1**. Furthermore, DFT calculations showed that **1-X** is an open core species where the $Co^{III}–X$ (X = F) and $Co^{IV}–O$ moieties are preferably in a *trans* configuration. The unpaired spin is heavily delocalized in the $Co^{IV}–O$ unit, providing the terminal oxygen with a partial radical character. According to our calculations, **1-X** has a more favorable

thermodynamic driving force and a smaller activation barrier than **1** to carry out C–H bond activation reactions, making **1-X** a much stronger oxidant both thermodynamically and kinetically. Notably, **1-X** is million-fold faster than **1** to oxidize ethylbenzene, and is at least four orders of magnitude more reactive than its diiron open core analogs to oxidize other substrates. Our findings indicated that the diamond core isomerization is likely a practical enzymatic strategy to unmask the strong oxidizing power of sMMO-**Q** necessary to attack the highly inert C–H bonds of methane.

Results and Discussion.

As we previously reported, the $Co_2^{III,IV}(\mu\text{-}O)_2$ diamond core complex **1** is able to cleave sp^3 C-H bonds as strong as those in ethylbenzene (BDE = 87 kcal/mol) with a second-order rate constant k_2 = 0.025(2) M^{-1} s^{-1} measured at -60 °C. In order to study the effect of Lewis bases, we first selected fluoride ion (F^-, pK_a = 3.17 in water) for our investigations. The addition of one equivalent of F^- (0.15 mM) into the methanol solution of **1** at -60 °C causes a 3-fold increase for the self-decay rate constant of **1** from 0.008 s^{-1} to 0.022 s^{-1}, suggesting that there is an interaction between **1** and F^-. In the presence of F^-, **1** reacts with excess ethylbenzene in a pseudo-first-order fashion with the reaction kinetics monitored at the characteristic 480 nm chromophore (Figure S1). No other intermediate was observed to form in the course of the reaction. As shown in Figure 1A, for each F^- concentration studied, the measured pseudo-first-order rate constant k_{obs} is linearly dependent on the concentration of ethylbenzene, indicating that the reaction is first-order with respect to the substrate. Moreover, the k_2 value (indicated by the slope of each linear plot in Figure 1A, see also Table S1) for ethylbenzene oxidation becomes higher when the concentration of F^- increases. With 5 equivalent of F^- present (0.75 mM), a 12-fold rate enhancement (0.31(3) M^{-1} s^{-1}) was observed. At a fixed ethylbenzene concentration, the reaction rate is linearly dependent on the concentration of F^- added (Figure S2), suggesting that the reaction is first-order for F^-. Thus, the reaction exhibited first-order dependence on all three reactants. For each F^- concentration studied, an H/D kinetic isotope effect (KIE) in the range of 4-10 was determined using deuterated ethylbenzene as the substrate (Figures S3-S5, Table S1), indicating that the cleavage of a C–H bond is the rate-determining step in the oxidation of ethylbenzene. Quantification of the oxidation product(s) of ethylbenzene by GC-MS indicated the formation of primarily acetophenone (34% yield, Table S2) and trace amount of 1-phenylethanol, accounting for ~60-70% of the oxidizing equivalents used after correcting for the formation yield of **1** (typically ~70%). No fluorinated product was observed. We further designed competitive experiments to measure H/D KIEs for ethylbenzene oxidations by reacting **1** with 1:1 mixture of PhEt and PhEt-d_{10} in the presence of different amount of F^- and analyzing the ratio of the non-deuterated/deuterated acetophenone. As shown in Table S1, the KIE values obtained in this method are consistent with those directly measured from kinetic rate constants.

We further extended our investigations to other Lewis bases with an increased basicity including NO_2^- (pK_a = 3.29 for a conjugate acid, all pK_a values in water), N_3^- (pK_a = 4.72), pyridine (pK_a = 5.3), CN^- (pK_a = 9.2) and OH^- (pK_a = 13.8). Notably, substrates having C–H bonds stronger than 87 kcal/mol such as toluene (BDE = 90 kcal/mol) can be oxidized by **1** in the presence of only one equivalent (0.15 mM) of any

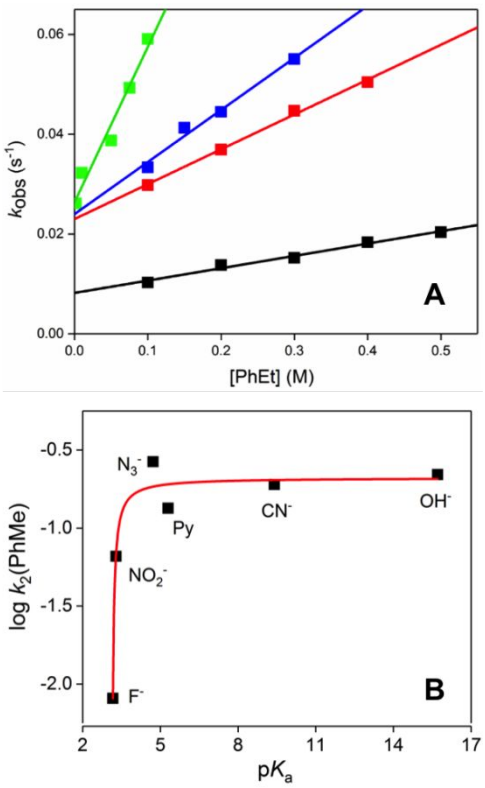

Figure 1. (A) Plots of k_{obs} as a function of the substrate concentration for ethylbenzene oxidation by 0.15 mM **1** in the presence of no F^- (black), 0.15 mM F^- (red), 0.45 mM F^- (blue) and 0.75 mM F^- (green) obtained in MeOH at -60 °C. The lines represent the best linear fittings. (B) Plot of log k_2(PhMe) as a function of the pK_a of the Lewis base for toluene oxidation by **1** in the presence of 1 equivalent of selected Lewis base in MeOH at -60 °C, fitted to a saturation curve.

Lewis base from this group studied. As shown in Figure 1B, the log k_2 for toluene oxidation exhibits a saturation behavior as a function of the pK_a of the Lewis base used. This observation suggests that at a fixed Lewis base concentration the maximum oxidizing power of **1** can be reached when the basicity of the Lewis base used is higher than the threshold pK_a ≈ 4. When deuterated toluene was used as the substrate, slower reactions were observed and H/D KIEs in the range of 1.6-10 were determined (1.1-10.8 from substrate competitive experiments, Figures S6-S11, Table S1), indicating that the rate-determining step for toluene oxidation is the cleavage of its C–H bond. For all Lewis bases studied, only oxygenated products (benzyl alcohol and benzaldehyde) were observed in the product analysis (Table S2). No functionalized product was identified.

With the introduction of a Lewis base having pK_a > 4 such as N_3^- in a stoichiometric amount (one equivalent, 0.15 mM), **1** is able to access strong C–H bonds up to those in methanol (BDE = 96 kcal/mol). A solvent KIE of 1.6 was determined using deuterated methanol as the solvent (Figure S12), suggesting that the self-decay of **1** in the presence of N_3^- is to oxidize the solvent methanol. In addition, tetrahydrofuran (THF, BDE = 92 kcal/mol) is oxidized to γ-butyrolactone and 2-hydroxytetrahydrofuran in a yield of 20% and 16%, respectively, with a rate of 0.085(4) M^{-1} s^{-1} and an H/D KIE of 5.4 (Figure S13). Furthermore, the rate for ethylbenzene oxidation by **1** in the presence of one equivalent (0.15 mM) of

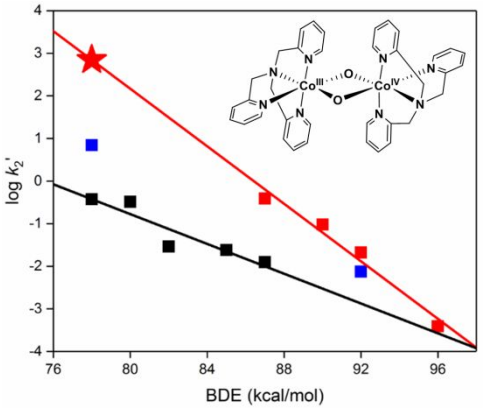

Figure 2. (A) Plots of log k_2' as a function of the C–H bond strength for substrate oxidations by **1** (black squares, data from ref. 10) and **1** + 0.15 mM N_3^- (red squares) in MeOH at -60 °C, and HO–Fe^{III}–O–Fe^{IV}=O in 3:1 CH_2Cl_2/MeCN at -80 °C (blue squares, data from ref. 9). The lines represent the best linear fittings. The red star represents the predicted rate for DHA oxidation by **1** + 0.15 mM N_3^-. Inset: schematic structure of the $Co^{III,IV}_2(\mu\text{-O})_2$ diamond core complex **1** studied in this work.

N_3^- exhibits a 30-fold increase as compared to the one by **1** only (Figure S14). Figure 2 shows that the log k_2' (k_2' = k_2/the number of equivalent hydrogen in the substrate) correlates linearly with the strength of the C–H bond being cleaved for **1** + N_3^- with a slope of -0.34. This slope is twice as big as the one observed for **1** without any added Lewis base in our previous work (-0.17).[18] The different sensitivity of the reaction rates to the C–H bond strength for these two systems (**1** + N_3^- *vs.* **1**), as well as that **1** + N_3^- is able to cleave C–H bonds stronger than 87 kcal/mol, strongly indicate that a new species, **1-X**, that is more powerful than the diamond core complex **1** in cleaving sp^3 C–H bonds is generated upon the interaction of a Lewis base X with **1**.

We hypothesized that **1-X** is an open core species X–Co^{III}–O–Co^{IV}–O, as analogous to the diiron system.[15,17] The conversion between **1** and **1-X** must be a fast equilibrium that disfavors the formation of **1-X** because 1) C–H bond cleavage is the rate-determining step, and 2) the formation of a detectable intermediate assignable to **1-X** was not observed on the UV-vis spectroscopy regardless of the identity and the amount of the Lewis base added. We noticed that the previously reported diiron open core species show only an absorption at ~400 nm but also lack intense and well-defined features in the visible to near-IR region.[15,17] On the other hand, the intense absorption of **1** at 480 nm provides a convenient way to measure the equilibrium constant K_{eq} for the conversion between **1** and **1-X** upon titrating a Lewis base of varied concentrations into the solution of **1**. We selected pyridine (py) as the Lewis base for this study because of its high enough basicity and high solubility in methanol even at -80 °C. For each pyridine concentration studied, we monitored the immediate decrease of the 480 nm band after the addition of the pyridine solution, recorded its absorbance after a well-mixed solution was obtained but before significant self-decay was observed, and used it to calculate the percentage of the remaining **1** in the solution after the equilibrium is established. As clearly shown in Figure 3, the fraction of the remaining **1** becomes smaller as the pyridine concentration increases, as expected. The titration data can be nicely fitted using a reciprocal model, allowing K_{eq} = 0.31(4) M^{-1} to be obtained

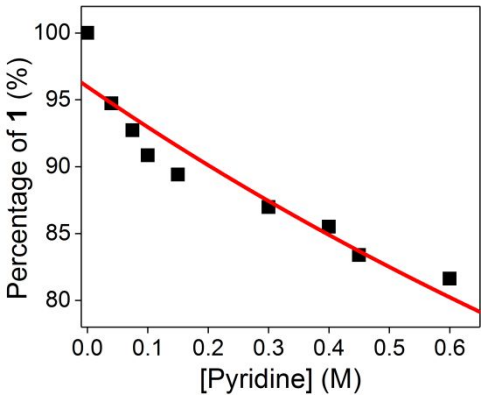

Figure 3. Plot of the percentage of the remaining **1** (initial concentration 0.15 mM) in titration experiments as a function of the concentration of pyridine added into the solution of **1**, fitted using a reciprocal model (red curve, see SI for more details).

(see Supporting Information for more details). Such a small K_{eq} value confirms that the equilibrium indeed disfavors the formation of **1-X**, for example, ~3.2 M pyridine is required in order to obtain a 50% formation yield of **1-X**. Under our typical experimental conditions for C–H bond oxidation (Lewis base concentration <0.1 M) **1-X** is only formed in a yield of <3%. Furthermore, the saturation behavior of the toluene oxidation rate as a function of the Lewis base pK_a (Figure 1B) strongly suggests that the K_{eq} values for Lewis bases having pK_a > 4 are quite similar.

The formation of a high-valent open core species X–Co^{III}–O–Co^{IV}–O (**1-X**) is of particular fundamental interest; therefore we spent significant effort trying to trap this highly reactive intermediate for spectroscopic characterizations. Our attempt to obtain its UV-vis spectrum was unsuccessful. Also, based on the K_{eq} value measured, it is unlikely that **1-X** can be obtained in high yields for characterization using X-ray absorption spectroscopy. Alternatively, we sought to investigate **1-X** using EPR spectroscopy. For similar considerations as in our titration experiments, pyridine was selected as the Lewis base for this study. X-band EPR spectra of samples containing **1** or **1-py** are shown in Figure 4. The spectrum of **1** (Figure 4A) generated upon one-electron oxidation of 1 mM $Co_2^{III}(\mu\text{-O})_2$ precursor is identical to that reported previously and represents ~70% formation yield of the $Co_2^{III,IV}(\mu\text{-O})_2$ diamond core species.[18] Upon the addition of a large excess pyridine (0.1 M and 0.3 M, respectively, for the spectra obtained in Figure 4B and 4C), a new feature was found to develop at g = ~2.15 with clearly visible hyperfine splittings due to the ^{59}Co nuclear spin (I = 7/2, natural abundance 100%). We assign this feature to **1-py**. The relative ratio of the signal intensities at g = ~2.15 vs. g = ~2 increases as the amount of pyridine added to the solution becomes higher, indicating that the conversion of **1** to **1-py** is positively dependent on the concentration of pyridine in the solution. This observation is consistent with the model of fast equilibrium between **1** and **1-py** described above. We also measured the EPR spectrum of a sample containing **1** treated with F^- (Figure S15), which is highly similar to those of the samples treated with pyridine but showed a lower concentration of EPR active species. Therefore, we focused our discussion on the samples treated with pyridine.

We then performed spectrum subtraction to reveal the EPR signal associated with **1-py**. The direct subtraction of the

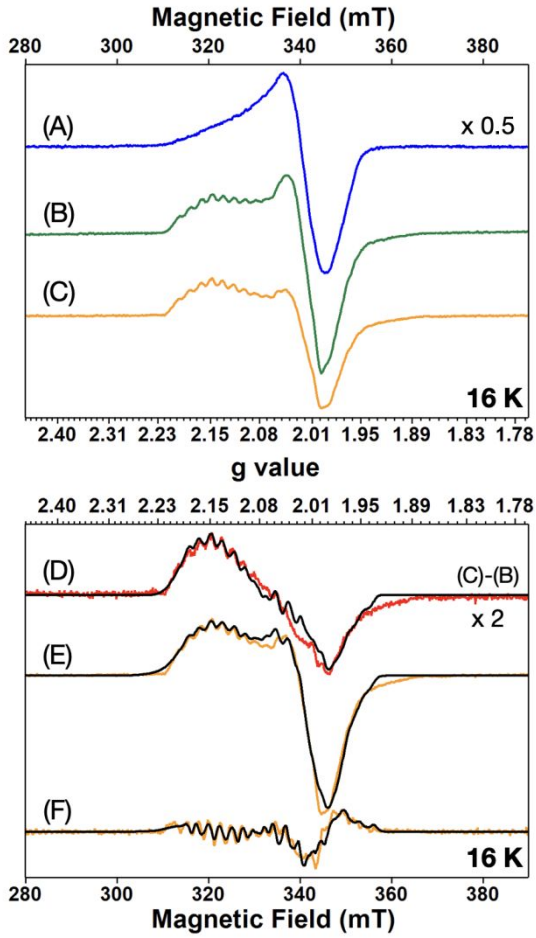

Figure 4. X-band EPR spectra of **1** and **1-py**. Top panel: the EPR spectrum of complex **1** (A); (B) a sample containing **1-py** obtained by treating complex **1** with 0.1 M pyridine; (C) a sample containing **1-py** obtained by treating complex **1** with 0.3 M pyridine. Bottom panel: (D) the difference spectrum between spectra (C) and (B) from the top panel (red), representing the EPR signal of **1-py**, and the corresponding simulation (black); (E) the same spectrum shown in (C) of the top panel (yellow) and the corresponding simulation (black) including the spectral components of **1-py** and **1**; (F) the 2nd derivative relative to the absorption spectrum of spectrum E (yellow) and its corresponding simulation (black). The simulation parameters for **1-py** are: g = [2.09, 2.08, 2.03], σ_g = [0.015, 0.004, 0.003], $A_1(^{59}\text{Co})$ = [120, 70, 90] MHz, $A_2(^{59}\text{Co})$ = [20, 50, 40] MHz. For **1**, the published simulation parameters are used (ref. 18). The measurement conditions are: microwave frequency 9.64 GHz, microwave power 2 μW, modulation frequency 100 kHz, modulation amplitude 1 mT, temperature 16 K.

spectrum shown in Figure 4A from that of Figure 4C always yielded unreasonable sharp line shape at g = ~2 resonance (see Figure S16). Instead, a more reasonable spectrum of **1-py** was obtained by subtracting the spectrum in Figure 4B from that of Figure 4C, which is shown in the bottom panel of Figure 4. To ensure a reliable spectral simulation, we simulated this difference spectrum (Figure 4D) together with the original spectrum in Figure 4C (shown also in Figure 4E together with its simulation). For the spectrum in Figure 4C, we included the parameters for describing both **1** and **1-py**. The parameters for **1** were fixed at the published values.[18] In this way, the simulation reproduced the spectral features representing **1-py** nicely (see Figure S17 for additional simulation results). To further illustrate the quality of the simulation, particularly the hyperfine splitting features, we took derivatives on both the spectrum and the corresponding simulation (effectively the 2nd derivative to the absorption spectrum) shown in Figure 4E and overlaid them together in Figure 4F. It shows that all the hyperfine splitting features are well reproduced by the simulation. The parameters obtained to describe the EPR signal of **1-py** are g_1 = 2.09, g_2 = 2.08, g_3 = 2.03, together with two different ^{59}Co A tensors (detailed parameters are listed in Figure 4 caption), indicating that **1-py** is an S = 1/2 species. The difference in the magnitude of the principle components in the two ^{59}Co A tensors (e.g. the magnitude of the largest component of one tensor is ~ 120 MHz, while of the other tensor is ~ 50 MHz) suggests that the spin density is more localized on one of the two Co sites of **1-py**. This is different from the diamond core complex **1**, where the spin density is equally distributed on both Co centers with two identical A tensors (see Table S5 for the comparison of the experimental determined and DFT predicted parameters).[18]

We then turned to DFT calculations to investigate the structure of **1-X** (X = F). Geometry optimization at the BP86/6-31G(D) + PCM(methanol) level provided low-spin ground states for both the diamond core complex **1** and the fluorine-bound open core complex **1-F**. **1-F** can exist in *cis* and *trans* isomeric forms, where the *trans* isomer is more stable than the *cis* isomer by 10.92 kcal/mol (Figures 5A and 5B). The calculated Co–O and Co–F distances for these two isomers are highly similar (Table S3). Interestingly, it was previously reported that the *trans* open core species was also the most stable isomer for the diiron analog (5.2 kcal/mol more stable than the *cis* isomer) supported by the same TPA ligand and with fluoride as the Lewis base.[15]

Of particular interest is the Co^{IV}–O moiety in *trans*-**1-F** where a terminal oxygen atom is bound to the Co(IV) center. The calculated Co^{IV}–O bond length of 1.74 Å is apparently longer than the one computed for the diiron analog (1.64 Å)[15] and those measured experimentally for Fe^{IV}=O complexes[19-20] and the only structurally characterized Co^{III}=O species (1.68 Å),[21] but is shorter than a Co^{IV}–O single bond.[22] Such a distance indicates that the Co^{IV}–O bond order is less than two but greater than one, and the oxygen atom has significant radical character. A recently characterized mononuclear Co^{IV}–O species by Nam and co-authors showed a similar Co^{IV}–O distance of 1.72 Å.[23] Supporting this notion is the calculated spin density population of *trans*-**1-F** (Figure 5C, Table S4), which shows that the spin density is largely distributed and delocalized on Co(IV) (+0.50) and the terminal oxygen atom (+0.35), suggesting that in *trans*-**1-F** the terminal oxygen has a partial radical character.

We also calculated the EPR parameters for both the diamond core (**1**) and open core (**1-X**, X = F, py) complexes (Table S5). The calculated g factors are in reasonable agreement with experimental values for both species. Furthermore, DFT predicted A values (for **1-py**, $A_1(^{59}\text{Co})$ = [158, -150, 100] MHz, $A_2(^{59}\text{Co})$ = [18, 0, -9] MHz) are in modest agreement with experiment, but successfully reproduced the pattern observed in EPR measurements.[22,24-26] Specifically, the diamond core complex **1** showed that the two cobalt centers have almost identical spin populations, indicating that **1** is a spin-delocalized species. On the other hand, the principal components of the two ^{59}Co A tensors calculated for complex **1-py** differ in the magnitude, which is

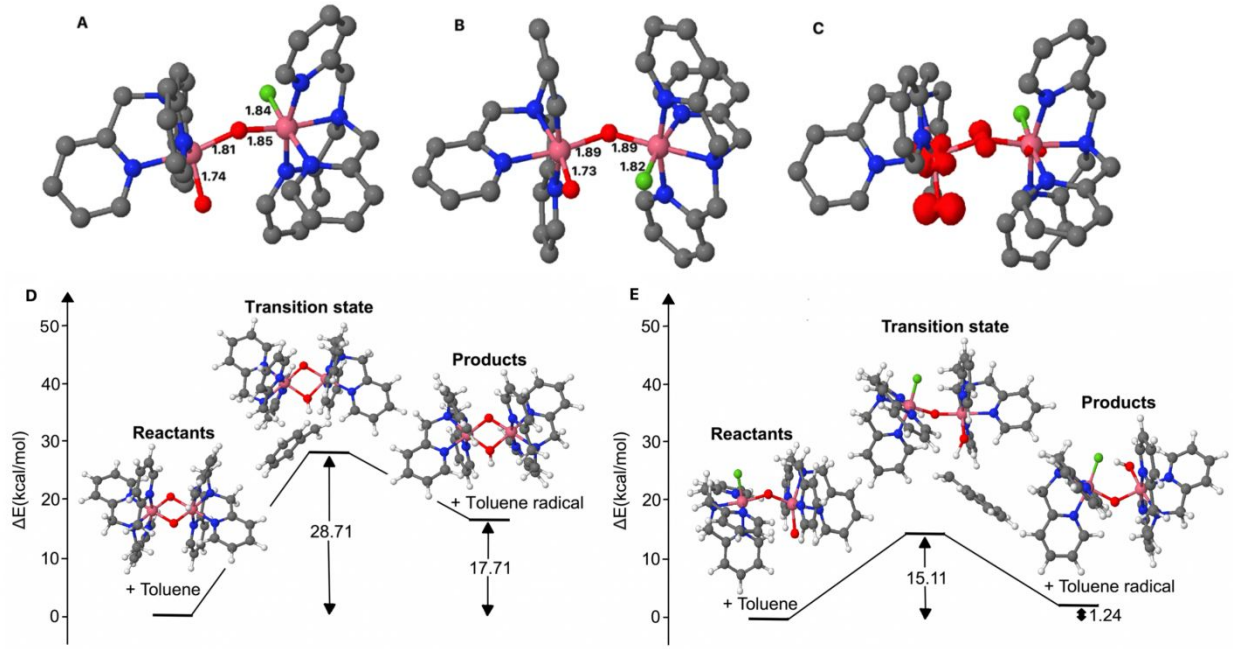

Figure 5. A, B: BP86/6-31G(D) + PCM(methanol) optimized structures for F–Co^{III}–O–Co^{IV}–O (**1-F**) in the *trans* (panel A) and *cis* (panel B) forms. Bond lengths are shown in Å for the selected bonds. **C**: Spin density plot of *trans*-**1-F**. **D**, **E**: Schematic depiction of the SCF potential energy changes for the transformations **1⟶2** (panel D) and **1-F⟶2-F** (panel E) and the structures of the corresponding reactants, transition states, and products. Pink, green, red, blue, and grey colors are used to depict Co, F, O, N, C atoms, respectively. Hydrogen atoms are omitted for clarity in panels A-C.

consistent with those obtained by EPR simulations and implies that the spin density is present more on one cobalt site than the other due to that these cobalt centers have different chemical environment. Therefore, DFT calculations support our assignment that **1-X** is an open core dicobalt(III,IV) species.

We further calculated the transition states of the C–H bond cleavage reactions by both **1** and **1-F** in order to better understand the reaction mechanism. According to calculations, conversion of **1** to Co^{III}(μ-O)(μ-OH)Co^{III} (**2**) by the hydrogen atom abstraction from toluene is energetically unfavorable with the enthalpy change of +17.71 kcal/mol (Figure 5D). The activation energy for the transformation **1⟶2** was computed to be 28.71 kcal/mol thus indicating unlikelihood of this reaction at a low temperature. This result is consistent with experimental observations that **1** is unable to cleave the C–H bond of toluene. In contrast, the hydrogen atom transfer from toluene to **1-F** with the formation of F–Co^{III}–O–Co^{III}–OH (**2-F**) has an enthalpy change of only +1.24 kcal/mol, which is 16.47 kcal/mol lower in energy than that of a similar transformation **1⟶2**. The complex **2-F** also shows a *cis*/*trans* isomerism, with the *cis* isomer being more stable by 2.85 kcal/mol due to a hydrogen bond interaction between the Co^{III}–F and Co^{III}–OH moieties (Figure 5E). For the transformation **1-F⟶2-F** the computed activation energy was found to be 15.11 kcal/mol, which is 13.60 kcal/mol lower than that for the transformation **1⟶2** (Figure 5E). Similar calculations using hydroxide ion instead of the fluoride ion showed that the conversion of HO–Co^{III}–O–Co^{IV}–O (**1-OH**) to HO–Co^{III}–O–Co^{III}–OH (**2-OH**) upon reacting with toluene has an enthalpy change of +4.53 kcal/mol and an activation barrier of 16.03 kcal/mol, which is lower in energy by 13.18 kcal/mol and 12.68 kcal/mol, respectively, than the conversion of **1** to **2** in the first pathway (Figure S18). Similar results were obtained using a different density functional B3LYP (see the SI for details). Thus, the DFT calculations suggest that the presence of a Lewis base can both increase the thermodynamic driving force and lower the activation barrier of the hydrogen atom transfer from a substrate to the dicobalt complex.

Based on our calculations, the electronic spin density appears to contribute to the high-reactivity of *trans*-**1-F**. While the spin density of **1** is equally distributed on the Co_2(μ-O)$_2$ diamond core, the spin density of *trans*-**1-F** is primarily localized on Co(IV) (+0.50) and the terminal oxygen atom (+0.35), thus displaying a significant radical character on the terminal oxygen atom (Figure 5C, Table S4). Therefore, hydrogen atom abstraction by the terminal oxygen in *trans*-**1-F** is much more feasible than **1** due to the completion of the octet during the reaction.[27] Our calculations further show that the highest occupied molecular orbital (HOMO) of *trans*-**1-F** (Figure S19) is higher in energy (-4.377 eV) as compared with the HOMO of **1** (-5.374 eV), making *trans*-**1-F** a higher energy hydrogen atom abstractor than **1**. Therefore, *trans*-**1-F** should have a more favorable thermodynamic driving force and a smaller activation barrier than **1** to carry out C–H bond activation reactions.

We propose a reaction mechanism shown in Scheme 1 that summarizes our experimental and computational findings. The interaction of the $Co_2^{III,IV}$(μ-O)$_2$ diamond core complex **1** with a Lewis base X produces a X–Co^{III}–O–Co^{IV}–O open core species **1-X** in a fast equilibrium, which strongly disfavors the formation of **1-X**. For Lewis bases having pK_a > 4, a small equilibrium constant K_{eq} = 0.31 M^{-1} was determined. Although present in only a small amount, **1-X** is capable of cleaving a C–H bond of the substrate in a rate-determining step with an *intrinsic second-order rate constant* k_{C-H}, generating a one-electron reduced species X–Co^{III}–O–Co^{III}–OH and a carbon radical. The oxygen rebound then yields the alcohol product, which can be further over-oxidized to form the ketone product.

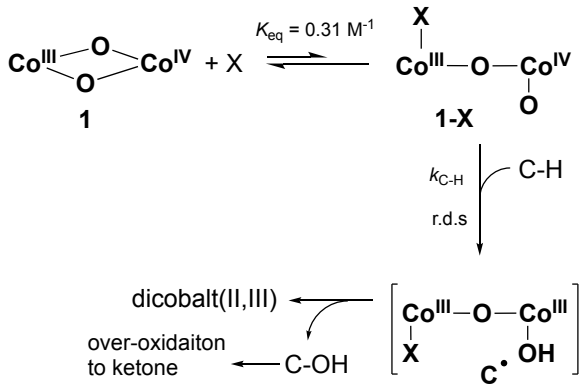

Scheme 1. Proposed mechanism for C-H bond oxidation by **1** in the presence of a Lewis base X.

For such a kinetic model that includes a fast equilibrium preceding a rate-determining step, the overall reaction rate should follow saturation kinetics, as expressed in eq. 1:

$$\text{rate} = \frac{k_{C-H}[X][\mathbf{1}][\text{substrate}]}{\frac{1}{K_{eq}} + [X]} = \frac{K_{eq}k_{C-H}[X][\mathbf{1}][\text{substrate}]}{1 + K_{eq}[X]} \quad (1)$$

where [X], [**1**] and [substrate] are the concentrations of the Lewis base X, complex **1** and the substrate, respectively. A saturated rate constant should be expected at high enough Lewis base concentrations. However, in our system, the reaction rates start to become too fast to be measured accurately when gradually increasing [X]. These measurable rates are still far below the one at the saturation level. Within this range of [X], $K_{eq}[X] << 1$, so eq. 1 can be simplified as eq. 2:

$$\text{rate} = K_{eq}k_{C-H}[X][\mathbf{1}][\text{substrate}] \quad (2)$$

Under pseudo-first-order conditions:

$$k_{obs} = K_{eq}k_{C-H}[X][\text{substrate}] \quad (3)$$

Eq. 3 is consistent with our observations that the measured k_{obs} is linearly dependent on the concentrations of the Lewis base (Figures S2 and S18) and the substrate (Figures S3-S14). For each substrate, the k_2 value determined is the product of K_{eq}, k_{C-H} and [X] (eq. 4).

$$k_2 = K_{eq}k_{C-H}[X] \quad (4)$$

k_{C-H} can then be obtained by rearranging eq. 4. For those measurements using a Lewis base having $pK_a > 4$ ($K_{eq} = 0.31$ M^{-1}) with a known concentration (typically [X] = 0.15 mM, see Table S1),

$$k_{C-H} = k_2/(K_{eq}\bullet[X]) = 2.15\times10^4\bullet k_2 \quad (5)$$

As clearly shown by eq. 5, the intrinsic rate constant k_{C-H} for each substrate oxidation by **1-X** is four orders of magnitude higher than the k_2 value measured. For example, k_{C-H} = 1.7×10^4 M^{-1} s^{-1} for ethylbenzene oxidation by **1-X** was calculated according to eq. 5. Compared to the rate of 0.025 M^{-1} s^{-1} by complex **1**, the rate enhancement upon opening up the diamond core is about a million-fold. For toluene, THF and methanol the corresponding k_{C-H} values are 6.2×10^3 M^{-1} s^{-1}, 1.8×10^3 M^{-1} s^{-1} and 8.6 M^{-1} s^{-1} (Table 1).

Our results revealed that the dicobalt open core species **1-X** is a much stronger oxidant than its diiron analogs supported by the same TPA ligand. As shown in Table 1, in the presence of only 0.15 mM N_3^-, the rate for ethylbenzene oxidation (0.78(3) M^{-1} s^{-1}) at -60 °C is more than three orders of magnitude higher than that (2×10^{-4} M^{-1} s^{-1}) of $Fe^{III,IV}_2(\mu\text{-}O)_2$ at -30 °C in the presence of 1 M H_2O,[16] Furthermore, the predicted DHA oxidation rate constant by **1-X** is ~2700 M^{-1} s^{-1} by extrapolating the linear fitting of the BDE plot to 78 kcal/mol (Figure 2). This rate is too fast to be measured experimentally, but should be about two orders of magnitude higher than that (28 M^{-1} s^{-1}) of $HO\text{–}Fe^{III}\text{–}O\text{–}Fe^{IV}\text{=}O$ and 8-fold higher than that (360 M^{-1} s^{-1}) of $CH_3O\text{–}Fe^{III}\text{–}O\text{–}Fe^{IV}\text{=}O$.[17] In addition, **1-X** oxidizes THF at a rate (0.085(4) M^{-1} s^{-1}) similar to that of $HO\text{–}Fe^{III}\text{–}O\text{–}Fe^{IV}\text{=}O$ (0.03 M^{-1} s^{-1}).[17] As described above, these rates are expected to increase further when the Lewis base is present in a higher concentration. Using the calculated k_{C-H} values of **1-X** for an estimate, **1-X** is at least four orders of magnitude more reactive than its diiron analogs.

Lewis bases have been shown in a number of studies capable of modulating C–H bond activation, electron transfer and oxygen atom transfer reactivities for high-valent mononuclear metal-oxo complexes in both heme and nonheme systems.[9-14] Upon coordinating to the metal center *cis*- or *trans*- to the oxo group, these Lewis bases tune both the geometric and electronic structures of the metal-oxo moieties and subsequently impact their redox properties and reactivities without altering the identities of these metal-oxo oxidants.[13-14,28-29] In contrast, for high-valent dinuclear diamond core complexes described for iron[15-17] and cobalt (present work), the interaction of a Lewis base with the dinuclear species changes the nature of the oxidant from bis-μ-oxo bridged diamond core to an open core with a terminal metal-oxo moiety. This conversion appears to have a greater effect on the C–H bond activation reactivities for these dinuclear diamond core complexes (10^6 fold rate enhancement) compared to the mononuclear counterparts (up to 10^4 fold rate enhancement).[12-13]

Table 1. Comparison of second-order rate constants (M^{-1} s^{-1}) for substrate oxidations by diamond core and open core diiron and dicobalt complexes.

Complex	Substrate					Ref
	DHA	PhEt	PhMe	THF	MeOH	
$Fe^{III,IV}_2(\mu\text{-}O)_2$	10^{-5}	2×10^{-4} [a]	1.2×10^{-4} [a]			16
1	1.5	2.5×10^{-2}				18
$HO\text{–}Fe^{III}\text{–}O\text{–}Fe^{IV}\text{=}O$	2.8×10^1			3×10^{-2}		17
$CH_3O\text{–}Fe^{III}\text{–}O\text{–}Fe^{IV}\text{=}O$	3.6×10^2					16
1 + 0.15 mM N_3^-	2.7×10^3 [b]	7.8×10^{-1}	2.9×10^{-1}	8.5×10^{-2}	1.2×10^{-3}	This work
1-X[c]		1.7×10^4	6.2×10^3	1.8×10^3	8.6	This work

[a] In the presence of 1 M H_2O.
[b] Estimated by extrapolating the linear fitting of the BDE plot shown in Figure 2.
[c] The rates for **1-X** (k_{C-H}) are calculated using the equation $k_{C-H} = k_2/(K_{eq}\bullet[X])$, where k_2 values are measured at a known [X] (such as 0.15 mM N_3^-). $K_{eq} = 0.31$ M^{-1} for Lewis bases having $pK_a > 4$.

The characterization of **1-X**, an open core species with a terminal Co^{IV}–O moiety, by EPR spectroscopy and DFT calculations is promising. As predicted by classic bonding theory,[30-31] such Co^{IV}–O species should be highly reactive. Our observation that **1-X** is able to access strong sp^3 C–H bonds at -60 °C with fast intrinsic rate constants is in accordance with such theoretical prediction. This high reactivity for an oxocobalt species has only been reported in the gas phase,[32] but has yet to be observed for mononuclear Co^{IV}–O and Co^{III}=O complexes that have been characterized in the condensed phase to date,[21,23,33-34]

Our findings are thus insightful for better understanding the high-valent diiron(IV) intermediate **Q** in sMMO. The attack of a highly inert C–H bond of methane directly by a diamond core species is unlikely. Instead, a thermodynamically and kinetically more potent open core species can be formed by the core isomerization equilibrium when necessary, for example, when the appropriate substrate is present. The level of the oxidizing power can be further tuned by the degree of such equilibrium. This is an excellent strategy to achieve substrate specificity and to avoid attacking residues having weaker C–H bonds.

Conclusion.

We have shown in the current study that the C–H bond cleaving reactivity of the $Co^{III,IV}_2(\mu\text{-}O)_2$ diamond core complex **1** can be dramatically enhanced when introducing a small amount of moderate or strong Lewis base into the solution of **1**. The interaction of **1** with a Lewis base opens up the diamond core through core isomerization equilibrium to generate an open core species **1-X**, which was characterized by EPR spectroscopy and DFT calculations as an S = 1/2 dicobalt(III,IV) species with a terminal Co^{IV}–O moiety. The equilibrium strongly disfavors the formation of **1-X**, with an equilibrium constant K_{eq} = 0.31 M^{-1} determined for Lewis bases having pK_a > 4. **1-X** is a much stronger oxidant than **1** to 1) afford million-fold rate enhancement for ethylbenzene oxidation and 2) cleave stronger C–H bonds up to 96 kcal/mol. Moreover, **1-X** is at least four orders of magnitude more reactive than its diiron analogs. Our results thus represented an important breakthrough in our effort aiming to develop more effective bio-inspired approaches for C–H bond activation. These findings are insightful for understanding the diiron(IV) intermediate sMMO-**Q**. Together with a similar rate enhancement reported previously for the diiron open core analogs, we suggest that the diamond core isomerization to release a thermodynamically and kinetically more potent oxidant is a practical strategy to target specific substrate with highly inert C–H bonds and to avoid unnecessary damage to other enzymatic residues.

ASSOCIATED CONTENT

Supporting Information

Experimental methods, computational details, Figures S1-S20, Table S1-S6. The Supporting Information is available free of charge on the ACS Publications website.

AUTHOR INFORMATION

Corresponding Author

*E-mail: dong1.wang@umontana.edu; talipovm@nmsu.edu; ysguo@andrew.cmu.edu

ACKNOWLEDGMENT

Support of this work was provided by the Center for Biomolecular Structure and Dynamics CoBRE (Grant NIGMS P20GM103546) and the University of Montana (Y.L. and D.W.). M.R.T. and S.H. were supported by New Mexico State University. The computational part of this work was supported by the Extreme Science and Engineering Discovery Environment (XSEDE) TG-CHE170004. J.X. and Y.G. acknowledge the support from NSF (CHE-1654060). We also thank Prof. Michael Hendrich at Carnegie Mellon University for valuable discussion on the EPR simulations.

REFERENCES

(1) Jasniewski, A. J.; Que, L., Jr. Dioxygen Activation by Nonheme Diiron Enzymes: Diverse Dioxygen Adducts, High-Valent Intermediates, and Related Model Complexes. *Chem. Rev.* **2018**, *118*, 2554-2592.

(2) Friedle, S.; Reisner, E.; Lippard, S. J. Current Challenges of Modeling Diiron Enzyme Active Sites for Dioxygen Activation by Biomimetic Synthetic Complexes *Chem. Soc. Rev.* **2010**, *39*, 2768-2779.

(3) Liu, K. E.; Wang, D.; Huynh, B. H.; Edmondson, D. E.; Salifoglou, A.; Lippard, S. J. Spectroscopic Detection of Intermediates in the Reaction of Dioxygen with the Reduced Methane Monooxygenase Hydroxylase from Methylococcus capsulatus (Bath). *J. Am. Chem. Soc.* **1994**, *116*, 7465-7466.

(4) Lee, S.-K.; Fox, B. G.; Froland, W. A.; Lipscomb, J. D.; Münck, E. A Transient Intermediate of the Methane Monooxygenase Catalytic Cycle Containing an $Fe^{IV}Fe^{IV}$ Cluster. *J. Am. Chem. Soc.* **1993**, *115*, 6450-6451.

(5) Shu, L.; Nesheim, J. C.; Kauffmann, K.; Münck, E.; Lipscomb, J. D.; Que, L., Jr. An $Fe^{IV}_2O_2$ Diamond Core Structure for the Key Intermediate Q of Methane Monooxygenase. *Science* **1997**, *275*, 515-518.

(6) Banerjee, R.; Proshlyakov, Y.; Lipscomb, J. D.; Proshlyakov, D. A. Structure of the Key Species in the Enzymatic Oxidation of Methane to Methanol. *Nature* **2015**, *518*, 431-435.

(7) Cutsail, G. E., III.; Banerjee, R.; Zhou, A.; Que, L., Jr.; Lipscomb, J. D.; DeBeer, S. High-Resolution Extended X-ray Absorption Fine Structure Analysis Provides Evidence for a Longer Fe···Fe Distance in the Q Intermediate of Methane Monooxygenase. *J. Am. Chem. Soc.* **2018**, *140*, 16807-16820.

(8) Castillo, R. G.; Banerjee, R.; Allpress, C. J.; Rohde, G. T.; Bill, E.; Que, L., Jr.; Lipscomb, J. D.; DeBeer, S. High-Energy-Resolution Fluorescence-Detected X-ray Absorption of the Q Intermediate of Soluble Methane Monooxygenase. *J. Am. Chem. Soc.* **2017**, *139*, 18024-18033.

(9) Fukuzumi, S.; Kotani, H.; Suenobu, T.; Hong, S.; Lee, Y.-M.; Nam, W. Contrasting Effects of Axial Ligands on Electron-Transfer Versus Proton-Coupled Electron-Transfer Reactions of Nonheme Oxoiron(IV) Complexes. *Chem. Eur. J.* **2010**, *16*, 354-361.

(10) Kang, Y.; Chen, H.; Jeong, Y. J.; Lai, W.; Bae, E. H.; Shaik, S.; Nam, W. Enhanced Reactivities of Iron(IV)-Oxo Porphyrin π-Cation Radicals in Oxygenation Reactions by Electron-Donating Axial Ligands. *Chem. Eur. J.* **2009**, *15*, 10039-10046.

(11) Sastri, C. V.; Lee, J.; Oh, K.; Lee, Y. J.; Lee, J.; Jackson, T. A.; Ray, K.; Hirao, H.; Shin, W.; Halfen, J. A.; Kim, J.; Que, L., Jr.; Shaik, S.; Nam, W. Axial ligand tuning of a nonheme iron(IV)-oxo unit for hydrogen atom abstraction. *Proc. Natl. Acad. Sci. USA* **2007**, *104*, 19181-19186.

(12) Neu, H. M.; Yang, T.; Baglia, R. A.; Yosca, T. H.; Green, M. T.; Quesne, M. G.; de Visser, S. P.; Goldberg, D. P. Oxygen-Atom Transfer Reactivity of Axially Ligated Mn(V)−Oxo Complexes: Evidence for Enhanced Electrophilic and Nucleophilic Pathways. *J. Am. Chem. Soc.* **2014**, *136*, 13845-13852.

(13) Prokop, K. A.; de Visser, S. P.; Goldberg, D. P. Unprecedented Rate Enhancements of Hydrogen-Atom Transfer to a Manganese(V)–Oxo Corrolazine Complex. *Angew. Chem. Int. Ed.* **2010**, *49*, 5091-5095.

(14) Takahashi, A.; Yamaki, D.; Ikemura, K.; Kurahashi, T.; Ogura, T.; Hada, M.; Fujii, H. Effect of the Axial Ligand on the Reactivity of the Oxoiron(IV) Porphyrin π-Cation Radical Complex: Higher Stabilization of the Product State Relative to the Reactant State. *Inorg. Chem.* **2012**, *51*, 7296-7305.

(15) Xue, G.; Geng, C.; Ye, S.; Fiedler, A. T.; Neese, F.; Que, L., Jr. Hydrogen-Bonding Effects on the Reactivity of [X-Fe^{III}-O-Fe^{IV}=O] (X = OH, F) Complexes toward C–H Bond Cleavage. *Inorg. Chem.* **2013**, *52*, 3976-3984.

(16) Xue, G.; Pokutsa, A.; Que, L., Jr. Substrate-Triggered Activation of a Synthetic [$Fe_2(\mu\text{-}O)_2$] Diamond Core for C–H Bond Cleavage. *J. Am. Chem. Soc.* **2011**, *133*, 16657-16667.

(17) Xue, G.; Hont, R. D.; Münck, E.; Que, L., Jr. Million-fold Activation of the [$Fe_2(\mu\text{-}O)_2$] Diamond Core for C–H Bond Cleavage. *Nat. Chem.* **2010**, *2*, 400-405.

(18) Li, Y.; Handunnetthige, S.; Farquhar, E. R.; Guo, Y.; Talipov, M. R.; Li, F.; Wang, D. Highly Reactive $Co^{III,IV}_2(\mu\text{-}O)_2$ Diamond Core Complex that Cleaves C–H Bonds. *J. Am. Chem. Soc.* **2019**, *141*, 20127-20136.

(19) Puri, M.; Que, L., Jr. Toward the Synthesis of More Reactive S = 2 Non-Heme Oxoiron(IV) Complexes. *Acc. Chem. Res.* **2015**, *48*, 2443-2452.

(20) Huang, X.; Groves, J. T. Beyond Ferryl-mediated Hydroxylation: 40 Years of the Rebound Mechanism and C–H Activation. *J. Biol. Inorg. Chem.* **2017**, *22*, 185-207.

(21) Goetz, M. K.; Hill, E. A.; Filatov, A. S.; Anderson, J. S. Isolation of a Terminal Co(III)-Oxo Complex. *J. Am. Chem. Soc.* **2018**, *140*, 13176-13180.

(22) Kwon, Y. M.; Lee, Y.; Evenson, G. E.; Jackson, T. A.; Wang, D. Crystal Structure and C−H Bond Cleaving Reactivity of a Mononuclear Co^{IV}-dinitrate Complex. *J. Am. Chem. Soc.* **2020**, *142*, 13435-13441.

(23) Wang, B.; Lee, Y.-M.; Tcho, W.-Y.; Tussupbayev, S.; Kim, S.-T.; Kim, Y.; Seo, M. S.; Cho, K.-B.; Dede, Y.; Keegan, B. C.; Ogura, T.; Kim, S. H.; Ohta, T.; Baik, M.-H.; Ray, K.; Shearer, J.; Nam, W. Synthesis and Reactivity of a Mononuclear Non-haem Cobalt(IV)-oxo Complex. *Nat. Commun.* **2017**, *8*, 14839.

(24) Harmer, J.; Doorslaer, S. V.; Gromov, I.; Broring, M.; Jeschke, G.; Schweiger, A. A Pulse EPR and ENDOR Investigation of the Electronic Structure of a σ-Carbon-Bonded Cobalt(IV) Corrole. *J. Phys. Chem. B* **2002**, *106*, 2801-2811.

(25) McAlpin, J. G.; Stich, T. A.; Ohlin, C. A.; Surendranath, Y.; Nocera, D. G.; Casey, W. H.; Britt, R. D. Electronic Structure Description of a [$Co(III)_3Co(IV)O_4$] Cluster: A Model for the Paramagnetic Intermediate in Cobalt-Catalyzed Water Oxidation. *J. Am. Chem. Soc.* **2011**, *133*, 15444-15452.

(26) Stich, T. A.; McAlpin, J. G.; Wall, R. M.; Rigsby, M. L.; Britt, R. D. Electron Paramagnetic Resonance Characterization of Dioxygen-Bridged Cobalt Dimers with Relevance to Water Oxidation. *Inorg. Chem.* **2016**, *55*, 12728-12736.

(27) Ye, S.; Neese, F. Nonheme oxo-iron(IV) intermediates form an oxyl radical upon approaching the C–H bond activation transition state. *Proc. Natl. Acad. Sci. USA* **2011**, *108*, 1228-1233.

(28) Jackson, T. A.; Rohde, J. U.; Seo, M. S.; Sastri, C. V.; De Hont, R.; Stubna, A.; Ohta, T.; Kitagawa, T.; Münck, E.; Nam, W.; Que, L., Jr. Axial Ligand Effects on the Geometric and Electronic Structures of Nonheme Oxoiron(IV) Complexes. *J. Am. Chem. Soc.* **2008**, *130*, 12394-12407.

(29) Rohde, J.-U.; Stubna, A.; Bominaar, E. L.; Münck, E.; Nam, W.; Que, L., Jr. Nonheme Oxoiron(IV) Complexes of Tris(2-pyridylmethyl)amine with cis-Monoanionic Ligands. *Inorg. Chem.* **2006**, *45*, 6435-6445.

(30) Winkler, J. R.; Gray, H. B. Electronic Structures of Oxo-Metal Ions. *Struct. Bond.* **2012**, *142*, 17-28.

(31) Ballhausen, C. J.; Gray, H. B. The Electronic Structure of the Vanadyl Ion. *Inorg. Chem.* **1962**, *1*, 111-122.

(32) Andris, E.; Navratil, R.; Jasik, J.; Srnec, M.; Rodriguez, M.; Costas, M.; Roithova, J. M-O Bonding Beyond the Oxo Wall: Spectroscopy and Reactivity of Cobalt(III)-Oxyl and Cobalt(III)-Oxo Complexes. *Angew. Chem. Int. Ed.* **2019**, *58*, 9619-9624.

(33) Hong, S.; Pfaff, F. F.; Kwon, E.; Wang, Y.; Seo, M.-S.; Bill, E.; Ray, K.; Nam, W. Spectroscopic Capture and Reactivity of a Low-Spin Cobalt(IV)-Oxo Complex Stabilized by Binding Redox-Inactive Metal Ions. *Angew. Chem. Int. Ed.* **2014**, *53*, 10403-10407.

(34) Goetz, M. K.; Anderson, J. S. Experimental Evidence for pKa-Driven Asynchronicity in C−H Activation by a Terminal Co(III)−Oxo Complex. *J. Am. Chem. Soc.* **2019**, *141*, 4051-4062.